2021/09/17
Archive Hash: 2fbc3ed-D
Archive Date: 2021/09/17

Search for long-lived particles decaying in the CMS endcap muon detectors in proton-proton collisions at $\sqrt{s} = 13\,\text{TeV}$

The CMS Collaboration

Abstract

A search for long-lived particles (LLPs) produced in decays of standard model (SM) Higgs bosons is presented. The data sample consists of $137\,\text{fb}^{-1}$ of proton-proton collisions at $\sqrt{s} = 13\,\text{TeV}$, recorded at the LHC in 2016–2018. A novel technique is employed to reconstruct decays of LLPs in the endcap muon detectors. The search is sensitive to a broad range of LLP decay modes and to masses as low as a few GeV. No excess of events above the SM background is observed. The most stringent limits to date on the branching fraction of the Higgs boson to LLPs subsequently decaying to quarks and $\tau^+\tau^-$ are found for proper decay lengths greater than 6, 20, and 40 m, for LLP masses of 7, 15, and 40 GeV, respectively.

Many extensions of the standard model (SM) predict the existence of neutral, weakly-coupled particles that have a long lifetime. These long-lived particles (LLPs) naturally arise in models of split supersymmetry (SUSY) [1–6], SUSY with weak R-parity violation [7–10], SUSY with gauge-mediated supersymmetry breaking [11–13], stealth SUSY [14, 15], hidden valley scenarios [16–18], baryogenesis triggered by weakly interacting massive particles [19–21], inelastic dark matter [22], and twin Higgs models [23–25].

In this Letter, we describe the first search at the LHC that uses a muon detector as a sampling calorimeter to identify showers produced by decays of LLPs. The CMS endcap muon detectors (EMD) are composed of detector planes interleaved with the steel layers of the magnet flux-return yoke. A schematic diagram of the EMD geometry is shown in Fig. 1. Decays of LLPs in the EMD induce hadronic and electromagnetic showers, giving rise to a high hit multiplicity in localized detector regions. The hadron calorimeter, solenoid magnet, and steel flux-return yoke together provide 20–27 nuclear interaction lengths of shielding, which is sufficiently large to suppress particle showers that are not fully contained (punch-through) to negligible levels.

This search has sensitivity to singly or multiply produced LLPs decaying to final states including hadrons, taus, electrons, or photons. The LLPs decaying to muons will very rarely produce a particle shower and will remain undetected by this search. We focus on a benchmark simplified model motivated by the twin Higgs scenario [16–18, 26–28] where the SM Higgs boson (H) decays to a pair of neutral long-lived scalars (S), each of which decays in turn to a pair of bottom quarks ($\mathrm{b\bar{b}}$), τ leptons ($\tau^+\tau^-$), or down quarks ($\mathrm{d\bar{d}}$). Further details of the simplified model can be found in Ref. [29]. The most stringent previous limit for mean proper decay lengths $c\tau < 0.3\,\mathrm{m}$ is based on a search for displaced jets in the CMS tracker [29]. For $c\tau > 0.3\,\mathrm{m}$, displaced vertices in the ATLAS muon spectrometer [30, 31] set the most stringent previous limit.

There are two inherent advantages of using the CMS EMD as a sampling calorimeter to detect LLPs over past searches that employ displaced vertices: (i) the absorber material in front of the EMD acts as a shield to maintain a sufficiently low level of background with the detection of a single LLP decay, a level that current displaced vertex searches can only achieve by requiring the detection of two LLP decays; (ii) the calorimetric nature of the particle shower, sensitive to the LLP energy rather than its mass, renders this search equally sensitive to all LLP masses considered, while vertex reconstruction efficiency tends to decrease with the LLP mass due to increasingly smaller opening angles.

Because of these advantages, the signal acceptance and sensitivity are improved relative to the previous best results [30, 31] by more than a factor of 6 (2) for an LLP mass of 7 GeV ($\geq$15) GeV and $c\tau > 100\,\mathrm{m}$. The improved signal acceptance that results from not requiring a second detected LLP decay is particularly powerful at very large $c\tau$, making the present search the first to be sensitive to LLP decays with $c\tau$ up to 1000 m and mass between 40 and 55 GeV for the Higgs boson to LLP decay branching fractions below 20%. Tabulated results and instructions to reproduce the signal efficiency are provided in HEPData [32].

The search is based on proton-proton (pp) collision data at 13 TeV collected during 2016–2018 at the CERN Large Hadron Collider (LHC), corresponding to an integrated luminosity of $137\,\mathrm{fb}^{-1}$. The central feature of the CMS experiment is a superconducting solenoid of 6 m internal diameter providing a magnetic field of 3.8 T. Located within the solenoid volume are a silicon pixel and strip tracker, a lead tungstate crystal electromagnetic calorimeter, and a brass and scintillator hadron calorimeter, each composed of a barrel and two endcap sections. Muons are detected in detectors embedded in the steel flux-return yoke outside the solenoid using three technologies: drift tubes (DTs) in the barrel, cathode strip chambers (CSCs) in the endcaps, and

resistive-plate chambers (RPCs) in the barrel and endcaps. Further details of the CMS detector and the coordinate system definition can be found in Ref. [33].

The CSC detector, which covers a region of pseudorapidity between $|\eta| = 0.9$ and 2.4 and plays a critical role for the search described in this Letter, is shown schematically in Fig 1. It is composed of four "stations" in each endcap, labeled ME1 to ME4, which are located approximately 7, 8, 9.5, and 10.5 m away from the interaction point along the beamline axis (z) on both ends of the detector, and are sandwiched between steel absorbers. Each chamber is composed of six thin layers containing cathode strips along the radial direction and anode wires perpendicular to the strips. Charged particles traversing the chambers ionize the gas molecules. The resulting electrons are accelerated towards the anode wires producing an avalanche, while the positive ions travel to the opposite end and induce signals in the cathode strips. By combining the information from signals on the anode wires and the cathode strips of each layer, we can determine the space-time coordinates of each such "hit" with a resolution of 400–500 μm and 5 ns [34].

The CMS event reconstruction is based on a particle-flow (PF) algorithm [35], which combines information from the tracker, calorimeters, and muon detectors to identify charged and neutral hadrons, photons, electrons, and muons, known collectively as PF candidates, which are clustered into jets using the anti-k_T algorithm with a distance parameter of 0.4 [36–38]. The transverse component of the negative vectorial sum of the momenta of all PF candidates is the missing transverse momentum $\vec{p}_T^{\,\text{miss}}$, and its magnitude is indicated as p_T^{miss}. The candidate vertex with the largest value of summed physics-object p_T^2 is taken to be the primary pp interaction vertex. The physics objects are the jets, clustered using the jet finding algorithm [37, 38] with the tracks assigned to candidate vertices as inputs, and the associated missing transverse momentum, taken as the negative vector sum of the p_T of those jets. The average neutral energy density from overlapping pp interactions (pileup) is estimated and subtracted from the reconstructed jet energies [39].

The simulated $H \to SS$ signal samples are generated using POWHEG 2.0 [40–43], and include gluon fusion, vector boson fusion, WH, ZH, and $t\bar{t}H$ production modes. The Higgs boson mass is set to 125 GeV, while the S mass (m_S) is set to 7, 15, 40, or 55 GeV. The $c\tau$ is varied between 1 mm and 100 m. Parton showering, hadronization, and the underlying event are modeled by PYTHIA 8.205 and 8.230 [44] with parameters set by the CUETP8M1 [45] and CP5 tunes [46] used for samples simulating the 2016 and 2017/18 datasets respectively. The NNPDF 3.0 [47] and 3.1 [48] parton distribution functions are used in the generation of all simulated samples. The GEANT4 [49] package is used to model the response of the CMS detector, and simulated minimum-bias events are mixed with the hard interactions in simulated events to match the observed pileup distribution in data.

An LLP that decays after it has traversed the calorimeter systems can produce large p_T^{miss} because its momentum will remain undetected, as p_T^{miss} is calculated solely from the tracker and calorimeter information. We exploit this feature by triggering on events with $p_T^{\text{miss}} > 120$ GeV [50], and subsequently requiring offline $p_T^{\text{miss}} > 200$ GeV. We require at least one jet with $p_T > 50$ GeV and pseudorapidity $|\eta| < 2.4$, because signal events passing the p_T^{miss} requirement are always produced together with a jet from initial-state radiation. To suppress backgrounds from W boson and top quark production, events containing an isolated electron (muon) passing loose identification criteria [51–53] with $p_T > 35$ (25) GeV and $|\eta| < 2.5$ (2.4) are vetoed.

The CSC hits are clustered in η and the azimuthal angle ϕ (in radians) using the DBSCAN algorithm [54], which groups hits by high-density regions. A minimum of 50 hits and a "distance parameter" of 0.2 is used. The geometric acceptance for at least one signal LLP of mass 7–

55 GeV decaying in the fiducial region of the CSC detectors ranges from 4–27% for $c\tau$ between 1–10 m, decreasing to 0.5–5% for $c\tau$ of 100 m. The efficiency for the showers to be reconstructed by the DBSCAN algorithm is approximately 80% for $b\bar{b}$ and $d\bar{d}$ decays and 65% for $\tau^+\tau^-$ decays. The accuracy of the simulation prediction for the cluster reconstruction efficiency relies on its ability to model correctly the response of the muon detectors in an environment with multiple particles, each producing a large number of secondary shower particles. This aspect is validated by measuring clusters produced in $Z \to \mu^+\mu^-$ data events where one of the muons undergoes bremsstrahlung in the EMD and the associated photon produces an electromagnetic shower, and the associated systematic uncertainty is taken into account in the overall uncertainty on the reconstruction efficiency.

The main SM backgrounds include punch-through jets, muons that undergo bremsstrahlung, and decays of SM LLPs, such as the neutral kaon K_L^0. To suppress background from punch-through jets or muon bremsstrahlung, we reject clusters that have a jet or muon within a $\Delta R = \sqrt{(\Delta\eta)^2 + (\Delta\phi)^2} < 0.4$ cone and with jet $p_T > 10$ GeV or muon $p_T > 20$ GeV. We veto clusters that have any hits in the two innermost rings of the ME1 station (ME1/1 and ME1/2), which have the least absorber material in front, or match any hit (with $\Delta R(\text{cluster, hit}) < 0.4$) in the RPCs located immediately next to ME1/2. In the region where the barrel and endcap muon detectors overlap ($0.8 < |\eta| < 1.2$), we veto any cluster matched to any track segment reconstructed in the innermost station of the DT detectors (MB1), or any hit in the RPCs situated in front of and behind MB1 matched to within $\Delta R(\text{cluster, segment/hit}) < 0.4$. Finally, we reject clusters with $|\eta| > 2.0$ to suppress the muon bremsstrahlung background that evaded the muon veto because of the high muon reconstruction and identification inefficiencies at larger $|\eta|$.

The inefficiencies for the jet, ME1, MB1, and RPC hit vetoes are predominantly caused by the presence of pileup particles and random noise, and are measured by randomly sampling the (η,ϕ) locations of clusters from the signal distribution and evaluating whether a jet or ME1/MB1/RPC hit has been observed within a $\Delta R < 0.4$ cone about the cluster's location, using $Z \to \mu^+\mu^-$ data events with the two muons from the Z decay removed. The loss of efficiency due to the muon veto is also affected by muon segments produced by particles resulting from the LLP decay itself. This contribution is further validated using a control sample of clusters matched to trackless jets made to resemble the signal LLP decay by requiring the neutral energy fraction to be larger than 95%. A 10% correction is applied to the signal efficiency to account for the simulation's mismodeling of the vetoes. To suppress noncollision backgrounds, we apply filters that remove events containing beam-halo muons or calorimeter noise [55]. To suppress background from cosmic ray muon showers, which produce hits in multiple regions of the CMS detector, we reject any event in which more than a quarter of DT and CSC ϕ-rings contain 50 or more hits. The efficiency for signal events to pass the ME1/1 and ME1/2 vetoes depends on the LLP decay location, and its average value is between 30–60% for the signal models considered. The efficiency for the remaining signal to pass all other vetoes is $\sim$80%.

After the veto requirements are applied, the dominant background source consists of decays of SM LLPs, which are predominantly produced by pileup interactions and are independent of the primary interaction that yielded the large p_T^{miss}. These pileup interactions can occur concurrently with the primary interaction (in-time pileup) or in adjacent bunch crossings (out-of-time or OOT pileup). Clusters produced by OOT pileup are rejected by requiring the cluster time (t_{cluster}), defined as the average time of the hits in the cluster relative to the LHC clock, to be consistent with an in-time interaction ($-5.0 < t_{\text{cluster}} < 12.5$ ns). A larger time window is used at positive values to capture signal clusters with longer delays from slower moving LLPs. The time window requirement suppresses the background by a factor of 5. An OOT

validation region (VR) is defined by selecting events containing clusters with $t_{\text{cluster}} \leq -5\,\text{ns}$, and is used to validate the background prediction method. To reject clusters composed of hits from multiple bunch crossings, we require that the root mean square spread of a cluster's hit times is less than 20 ns.

There are several features that distinguish between signal and background clusters. Clusters from all background processes occur more often at larger values of $|\eta|$, as the effectiveness of the jet and muon vetoes decrease because of increasing reconstruction inefficiencies. Signal clusters often occupy more than one CSC station and occur more frequently in stations further away from the primary interaction point. A cluster identification algorithm was devised that makes successively more restrictive $|\eta|$ requirements as the number of CSC stations containing hits and the distance between the station and the primary interaction point decrease. The cluster identification algorithm has ∼80% efficiency for clusters originating from S decays in the simulation, and suppresses the background by a factor of 3.

The events that pass the cluster identification criteria are used to define the search region, and those that fail are used as an additional in-time VR. The signal efficiency of the combined cluster reconstruction, veto, and identification selections is shown as a function of the simulated r and z decay positions of the particle S in Fig. 1. The combined efficiency averaged over the full region of the CSC detector is 15–30% for the signal models considered.

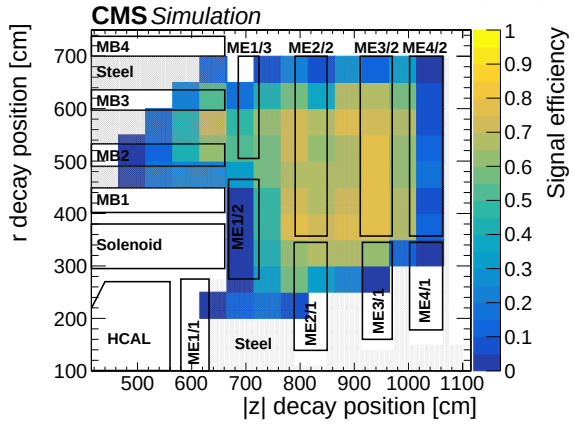

Figure 1: The signal efficiency of the combined cluster reconstruction, veto, and identification selections as a function of the simulated r and z decay positions of S decaying to $\text{b}\bar{\text{b}}$, for a mass of 15 GeV and a uniformly distributed mixture of events with $c\tau$ between 1–10 m. The barrel and endcap muon stations are drawn as black boxes and labeled by their station names, showing the geometry of the muon detectors. Regions occupied by the steel return yoke are shaded in gray.

The number of hits in the cluster (N_{hits}) and the azimuthal angle between the cluster location and the $\vec{p}_{\text{T}}^{\text{miss}}$ ($\Delta\phi_{\text{c}}$) are used to make the final discrimination between signal and background. The distribution of N_{hits} remains high at large N_{hits} values for signal events, but for background events the distribution of N_{hits} decreases sharply with increasing N_{hits} values. For signal, $\Delta\phi_{\text{c}}$ peaks near zero either because the $\vec{p}_{\text{T}}^{\text{miss}}$ results from the same S decay that produced the cluster or the large $p_{\text{T}}^{\text{miss}}$ requirement tends to select highly boosted Higgs bosons for which the S and H momentum vectors are spatially close to each other. For the backgrounds, $\Delta\phi_{\text{c}}$ is independent of N_{hits}, enabling the use of the matrix (ABCD) method to predict the background yield in the signal-enriched bin D as $N_{\text{D}} = (N_{\text{A}} N_{\text{C}})/N_{\text{B}}$, where N_{X} is the background event yield in each bin X. Bin A includes events with $\Delta\phi_{\text{c}} \geq 0.75$ and $N_{\text{hits}} > 130$; bin B includes events with $\Delta\phi_{\text{c}} \geq 0.75$ and $N_{\text{hits}} \leq 130$; bin C includes events with $\Delta\phi_{\text{c}} < 0.75$ and $N_{\text{hits}} \leq 130$; and bin

D includes events with $\Delta\phi_c < 0.75$ and $N_{hits} > 130$. The distributions of N_{hits} in bins C and D, and $\Delta\phi_c$ in bins A and D are shown in Fig. 2, for the data and for the signal assuming $S \to d\bar{d}$ decays with various S masses.

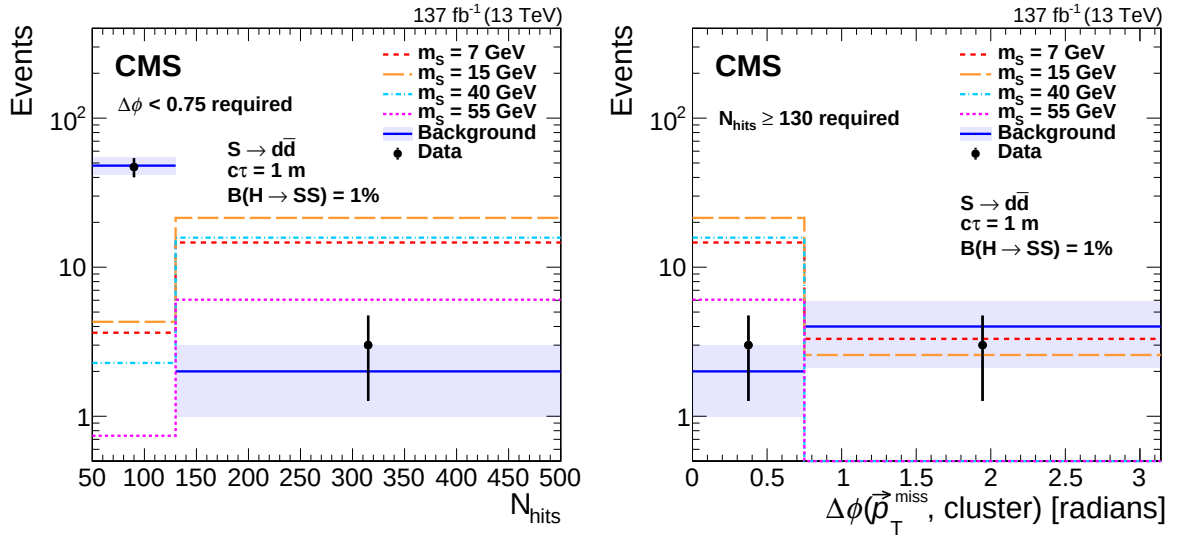

Figure 2: Distributions of N_{hits} (left) and $\Delta\phi_c$ (right) in the search region. The background predicted by the fit is shown in blue with the shaded region showing the fitted uncertainty. The expected signal with $\mathcal{B}(H \to SS) = 1\%$, $S \to d\bar{d}$, and $c\tau = 1\,m$ is shown for m_S of 7, 15, 40, and 55 GeV in various colors and dotted lines. The N_{hits} distribution includes only events in bins C and D, while the $\Delta\phi_c$ includes only events in bins A and D. The last bin in the N_{hits} distributions includes overflow events.

To account for a potential signal contribution to bins A, B, and C, a binned maximum likelihood fit is performed simultaneously in the four bins, with a common signal strength parameter scaling the signal yields in each bin. The background component of the fit is constrained to obey the ABCD relationship. Systematic uncertainties that affect the signal yield are missing higher order QCD corrections (21%), cluster reconstruction and identification efficiency (6%), veto efficiencies (4%), jet energy scale (4%) [56], simulation sample statistical uncertainties (3–5%), and luminosity (1.6%) [57–59]. These systematic uncertainties and the statistical uncertainty of the simulated signal samples are treated as nuisance parameters in the fit.

The background estimation procedure is validated using events in the OOT and in-time VRs, predicting 1.3 ± 0.6 and 1.4 ± 0.6 events respectively. In both VRs, 2 events are observed. In the signal-depleted A, B, and C bins of the search region, we observe 3, 96, and 47 events in the data, respectively. Using the fit procedure described above and assuming no signal contribution, we predict 2.0 ± 1.0 background events in the signal-enriched region D, and observe 3 events. The uncertainty in the background prediction is dominated by the statistical uncertainty in the event yields of the signal-depleted A, B, and C bins. No excess of events above the SM background is observed.

We evaluate 95% confidence level (CL) limits on the branching fraction $\mathcal{B}(H \to SS)$ using the modified frequentist criterion CL_s [60–62] with the profile likelihood ratio test statistic. The upper limits are shown in Fig. 3 for the $S \to d\bar{d}$ and $S \to \tau^+\tau^-$ decay modes, as a function of $c\tau$ for a selection of values of m_S. The exclusion limits for $S \to b\bar{b}$ are within 3% of the exclusion limits for $S \to d\bar{d}$ for $m_S > 2m_b$.

In summary, proton-proton collision data at $\sqrt{s} = 13\,TeV$ recorded by the CMS experiment in

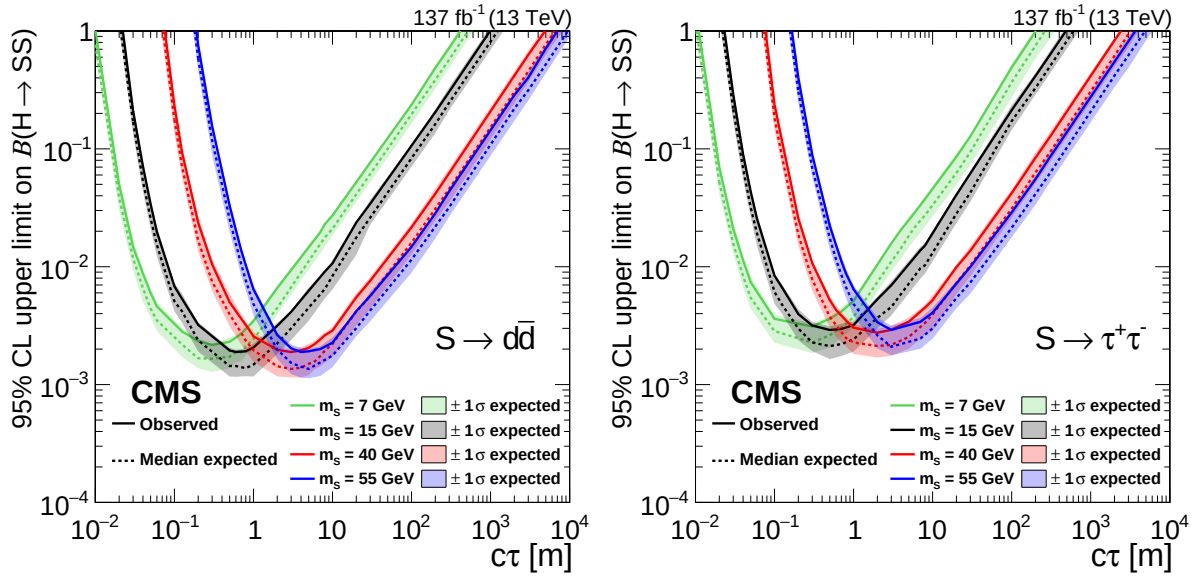

Figure 3: The 95% CL expected (dotted curves) and observed (solid curves) upper limits on the branching fraction $\mathcal{B}(\mathrm{H} \to \mathrm{SS})$ as functions of $c\tau$ for the $\mathrm{S} \to \mathrm{d\bar{d}}$ (left) and $\mathrm{S} \to \tau^+\tau^-$ (right) decay modes. The exclusion limits are shown for four different mass hypotheses: 7, 15, 40, and 55 GeV.

2016–2018, corresponding to an integrated luminosity of 137 fb^{-1}, have been used to conduct the first search for beyond the standard model (SM) long-lived particles (LLPs) using the CMS endcap muon detectors as a calorimeter. Based on a unique detector signature, the search is largely model-independent, with sensitivity to a broad range of LLP decay modes and to LLP masses as low as a few GeV. With the excellent shielding provided by the inner CMS detector, the background is suppressed to a low level and a search for a single LLP decay is possible. No significant deviation from the SM background is observed, and the most stringent limits on the branching fraction of Higgs boson to LLP decaying to $\mathrm{d\bar{d}}$, $\mathrm{b\bar{b}}$, and $\tau^+\tau^-$ are set for proper decay lengths $c\tau > 6$, 20, and 40 m, and LLP masses of 7, 15, and 40 GeV, respectively. For $c\tau > 100$ m, this search outperforms the previous best limits [30, 31] by a factor of 6 (2) for an LLP mass of 7 ($\geq$15) GeV.

Acknowledgments

We congratulate our colleagues in the CERN accelerator departments for the excellent performance of the LHC and thank the technical and administrative staffs at CERN and at other CMS institutes for their contributions to the success of the CMS effort. In addition, we gratefully acknowledge the computing centers and personnel of the Worldwide LHC Computing Grid and other centers for delivering so effectively the computing infrastructure essential to our analyses. Finally, we acknowledge the enduring support for the construction and operation of the LHC, the CMS detector, and the supporting computing infrastructure provided by the following funding agencies: BMBWF and FWF (Austria); FNRS and FWO (Belgium); CNPq, CAPES, FAPERJ, FAPERGS, and FAPESP (Brazil); MES (Bulgaria); CERN; CAS, MoST, and NSFC (China); MINCIENCIAS (Colombia); MSES and CSF (Croatia); RIF (Cyprus); SENESCYT (Ecuador); MoER, ERC PUT and ERDF (Estonia); Academy of Finland, MEC, and HIP (Finland); CEA and CNRS/IN2P3 (France); BMBF, DFG, and HGF (Germany); GSRT (Greece); NKFIA (Hungary); DAE and DST (India); IPM (Iran); SFI (Ireland); INFN (Italy); MSIP and NRF (Republic of Korea); MES (Latvia); LAS (Lithuania); MOE and UM (Malaysia); BUAP, CIN-

VESTAV, CONACYT, LNS, SEP, and UASLP-FAI (Mexico); MOS (Montenegro); MBIE (New Zealand); PAEC (Pakistan); MSHE and NSC (Poland); FCT (Portugal); JINR (Dubna); MON, RosAtom, RAS, RFBR, and NRC KI (Russia); MESTD (Serbia); SEIDI, CPAN, PCTI, and FEDER (Spain); MOSTR (Sri Lanka); Swiss Funding Agencies (Switzerland); MST (Taipei); ThEPCenter, IPST, STAR, and NSTDA (Thailand); TUBITAK and TAEK (Turkey); NASU (Ukraine); STFC (United Kingdom); DOE and NSF (USA).

References

[1] G. F. Giudice and A. Romanino, "Split supersymmetry", *Nucl. Phys. B* **699** (2004) 65, doi:10.1016/j.nuclphysb.2004.08.001, arXiv:hep-ph/0406088. [Erratum: doi:10.1016/j.nuclphysb.2004.11.048].

[2] J. L. Hewett, B. Lillie, M. Masip, and T. G. Rizzo, "Signatures of long-lived gluinos in split supersymmetry", *JHEP* **09** (2004) 070, doi:10.1088/1126-6708/2004/09/070, arXiv:hep-ph/0408248.

[3] N. Arkani-Hamed, S. Dimopoulos, G. F. Giudice, and A. Romanino, "Aspects of split supersymmetry", *Nucl. Phys. B* **709** (2005) 3, doi:10.1016/j.nuclphysb.2004.12.026, arXiv:hep-ph/0409232.

[4] P. Gambino, G. F. Giudice, and P. Slavich, "Gluino decays in split supersymmetry", *Nucl. Phys. B* **726** (2005) 35, doi:10.1016/j.nuclphysb.2005.08.011, arXiv:hep-ph/0506214.

[5] A. Arvanitaki, N. Craig, S. Dimopoulos, and G. Villadoro, "Mini-split", *JHEP* **02** (2013) 126, doi:10.1007/JHEP02(2013)126, arXiv:1210.0555.

[6] N. Arkani-Hamed et al., "Simply unnatural supersymmetry", 2012. arXiv:1212.6971.

[7] P. Fayet, "Supergauge invariant extension of the Higgs mechanism and a model for the electron and its neutrino", *Nucl. Phys. B* **90** (1975) 104, doi:10.1016/0550-3213(75)90636-7.

[8] G. R. Farrar and P. Fayet, "Phenomenology of the production, decay, and detection of new hadronic states associated with supersymmetry", *Phys. Lett. B* **76** (1978) 575, doi:10.1016/0370-2693(78)90858-4.

[9] S. Weinberg, "Supersymmetry at ordinary energies. Masses and conservation laws", *Phys. Rev. D* **26** (1982) 287, doi:10.1103/PhysRevD.26.287.

[10] R. Barbier et al., "*R*-parity violating supersymmetry", *Phys. Rept.* **420** (2005) 1, doi:10.1016/j.physrep.2005.08.006, arXiv:hep-ph/0406039.

[11] G. F. Giudice and R. Rattazzi, "Theories with gauge mediated supersymmetry breaking", *Phys. Rept.* **322** (1999) 419, doi:10.1016/S0370-1573(99)00042-3, arXiv:hep-ph/9801271.

[12] P. Meade, N. Seiberg, and D. Shih, "General gauge mediation", *Prog. Theor. Phys. Suppl.* **177** (2009) 143, doi:10.1143/PTPS.177.143, arXiv:0801.3278.

[13] M. Buican, P. Meade, N. Seiberg, and D. Shih, "Exploring general gauge mediation", *JHEP* **03** (2009) 016, doi:10.1088/1126-6708/2009/03/016, arXiv:0812.3668.

[14] J. Fan, M. Reece, and J. T. Ruderman, "Stealth supersymmetry", *JHEP* **11** (2011) 012, doi:10.1007/JHEP11(2011)012, arXiv:1105.5135.

[15] J. Fan, M. Reece, and J. T. Ruderman, "A stealth supersymmetry sampler", *JHEP* **07** (2012) 196, doi:10.1007/JHEP07(2012)196, arXiv:1201.4875.

[16] M. J. Strassler and K. M. Zurek, "Echoes of a hidden valley at hadron colliders", *Phys. Lett. B* **651** (2007) 374, doi:10.1016/j.physletb.2007.06.055, arXiv:hep-ph/0604261.

[17] M. J. Strassler and K. M. Zurek, "Discovering the Higgs through highly-displaced vertices", *Phys. Lett. B* **661** (2008) 263, doi:10.1016/j.physletb.2008.02.008, arXiv:hep-ph/0605193.

[18] T. Han, Z. Si, K. M. Zurek, and M. J. Strassler, "Phenomenology of hidden valleys at hadron colliders", *JHEP* **07** (2008) 008, doi:10.1088/1126-6708/2008/07/008, arXiv:0712.2041.

[19] Y. Cui, L. Randall, and B. Shuve, "A WIMPy baryogenesis miracle", *JHEP* **04** (2012) 075, doi:10.1007/JHEP04(2012)075, arXiv:1112.2704.

[20] Y. Cui and R. Sundrum, "Baryogenesis for weakly interacting massive particles", *Phys. Rev. D* **87** (2013) 116013, doi:10.1103/PhysRevD.87.116013, arXiv:1212.2973.

[21] Y. Cui and B. Shuve, "Probing baryogenesis with displaced vertices at the LHC", *JHEP* **02** (2015) 049, doi:10.1007/JHEP02(2015)049, arXiv:1409.6729.

[22] D. Smith and N. Weiner, "Inelastic dark matter", *Phys. Rev. D* **64** (2001) 043502, doi:10.1103/PhysRevD.64.043502, arXiv:hep-ph/0101138.

[23] Z. Chacko, H.-S. Goh, and R. Harnik, "Natural electroweak breaking from a mirror symmetry", *Phys. Rev. Lett.* **96** (2006) 231802, doi:10.1103/PhysRevLett.96.231802, arXiv:hep-ph/0506256.

[24] D. Curtin and C. B. Verhaaren, "Discovering uncolored naturalness in exotic Higgs decays", *JHEP* **12** (2015) 072, doi:10.1007/JHEP12(2015)072, arXiv:1506.06141.

[25] H.-C. Cheng, S. Jung, E. Salvioni, and Y. Tsai, "Exotic quarks in twin Higgs models", *JHEP* **03** (2016) 074, doi:10.1007/JHEP03(2016)074, arXiv:1512.02647.

[26] N. Craig, A. Katz, M. Strassler, and R. Sundrum, "Naturalness in the dark at the LHC", *JHEP* **07** (2015) 105, doi:10.1007/JHEP07(2015)105, arXiv:1501.05310.

[27] M. J. Strassler, "On the phenomenology of hidden valleys with heavy flavor", 2008. arXiv:0806.2385.

[28] J. E. Juknevich, D. Melnikov, and M. J. Strassler, "A pure-glue hidden valley I. states and decays", *JHEP* **07** (2009) 055, doi:10.1088/1126-6708/2009/07/055, arXiv:0903.0883.

[29] CMS Collaboration, "Search for long-lived particles using displaced jets in proton-proton collisions at $\sqrt{s} = 13$ TeV", 2020. arXiv:2012.01581. Submitted to *Phys. Rev. D*.

[30] ATLAS Collaboration, "Search for long-lived particles produced in pp collisions at $\sqrt{s} = 13$ TeV that decay into displaced hadronic jets in the ATLAS muon spectrometer", *Phys. Rev. D* **99** (2019) 052005, doi:10.1103/PhysRevD.99.052005, arXiv:1811.07370.

[31] ATLAS Collaboration, "Search for long-lived neutral particles produced in pp collisions at $\sqrt{s} = 13$ TeV decaying into displaced hadronic jets in the ATLAS inner detector and muon spectrometer", *Phys. Rev. D* **101** (2020) 052013, doi:10.1103/PhysRevD.101.052013, arXiv:1911.12575.

[32] "HEPData record for this analysis", 2021. doi:10.17182/hepdata.104408.

[33] CMS Collaboration, "The CMS experiment at the CERN LHC", *JINST* **3** (2008) S08004, doi:10.1088/1748-0221/3/08/S08004.

[34] CMS Collaboration, "Performance of the CMS cathode strip chambers with cosmic rays", *JINST* **5** (2010) T03018, doi:10.1088/1748-0221/5/03/T03018, arXiv:0911.4992.

[35] CMS Collaboration, "Particle-flow reconstruction and global event description with the CMS detector", *JINST* **12** (2017) P10003, doi:10.1088/1748-0221/12/10/P10003, arXiv:1706.04965.

[36] M. Cacciari and G. P. Salam, "Dispelling the N^3 myth for the k_T jet-finder", *Phys. Lett. B* **641** (2006) 57, doi:10.1016/j.physletb.2006.08.037, arXiv:hep-ph/0512210.

[37] M. Cacciari, G. P. Salam, and G. Soyez, "The anti-k_T jet clustering algorithm", *JHEP* **04** (2008) 063, doi:10.1088/1126-6708/2008/04/063, arXiv:0802.1189.

[38] M. Cacciari, G. P. Salam, and G. Soyez, "FastJet user manual", *Eur. Phys. J. C* **72** (2012) 1896, doi:10.1140/epjc/s10052-012-1896-2, arXiv:1111.6097.

[39] M. Cacciari and G. P. Salam, "Pileup subtraction using jet areas", *Phys. Lett. B* **659** (2008) 119, doi:10.1016/j.physletb.2007.09.077, arXiv:0707.1378.

[40] P. Nason, "A new method for combining NLO QCD with shower Monte Carlo algorithms", *JHEP* **11** (2004) 040, doi:10.1088/1126-6708/2004/11/040, arXiv:hep-ph/0409146.

[41] S. Frixione, P. Nason, and C. Oleari, "Matching NLO QCD computations with parton shower simulations: the POWHEG method", *JHEP* **11** (2007) 070, doi:10.1088/1126-6708/2007/11/070, arXiv:0709.2092.

[42] S. Alioli, P. Nason, C. Oleari, and E. Re, "A general framework for implementing NLO calculations in shower Monte Carlo programs: the POWHEG BOX", *JHEP* **06** (2010) 043, doi:10.1007/JHEP06(2010)043, arXiv:1002.2581.

[43] E. Re, "Single-top Wt-channel production matched with parton showers using the POWHEG method", *Eur. Phys. J. C* **71** (2011) 1547, doi:10.1140/epjc/s10052-011-1547-z, arXiv:1009.2450.

[44] T. Sjöstrand et al., "An introduction to PYTHIA 8.2", *Comput. Phys. Commun.* **191** (2015) 159, doi:10.1016/j.cpc.2015.01.024, arXiv:1410.3012.

[45] CMS Collaboration, "Event generator tunes obtained from underlying event and multiparton scattering measurements", *Eur. Phys. J. C* **76** (2016) 155, doi:10.1140/epjc/s10052-016-3988-x, arXiv:1512.00815.

[46] CMS Collaboration, "Extraction and validation of a new set of CMS PYTHIA8 tunes from underlying-event measurements", *Eur. Phys. J. C* **80** (2020) 4, doi:10.1140/epjc/s10052-019-7499-4, arXiv:1903.12179.

[47] NNPDF Collaboration, "Parton distributions for the LHC Run II", *JHEP* **04** (2015) 040, doi:10.1007/JHEP04(2015)040, arXiv:1410.8849.

[48] NNPDF Collaboration, "Parton distributions from high-precision collider data", *Eur. Phys. J. C* **77** (2017) 663, doi:10.1140/epjc/s10052-017-5199-5, arXiv:1706.00428.

[49] GEANT4 Collaboration, "GEANT4—a simulation toolkit", *Nucl. Instrum. Meth. A* **506** (2003) 250, doi:10.1016/S0168-9002(03)01368-8.

[50] CMS Collaboration, "The CMS trigger system", *JINST* **12** (2017) P01020, doi:10.1088/1748-0221/12/01/P01020, arXiv:1609.02366.

[51] CMS Collaboration, "Electron and photon reconstruction and identification with the CMS experiment at the CERN LHC", *JINST* **16** (2021) P05014, doi:10.1088/1748-0221/16/05/P05014, arXiv:2012.06888.

[52] CMS Collaboration, "Performance of the CMS muon detector and muon reconstruction with proton-proton collisions at $\sqrt{s} = 13$ TeV", *JINST* **13** (2018) P06015, doi:10.1088/1748-0221/13/06/P06015, arXiv:1804.04528.

[53] CMS Collaboration, "Performance of the reconstruction and identification of high-momentum muons in proton-proton collisions at $\sqrt{s} = 13$ TeV", *JINST* **15** (2020) P02027, doi:10.1088/1748-0221/15/02/P02027, arXiv:1912.03516.

[54] M. Ester, H.-P. Kriegel, J. Sander, and X. Xu, "A density-based algorithm for discovering clusters in large spatial databases with noise", in *Proceedings of the Second International Conference on Knowledge Discovery and Data Mining*, p. 226. Association for the Advancement of Artificial Intelligence, 1996.

[55] CMS Collaboration, "Missing transverse energy performance of the CMS detector", *JINST* **6** (2011) P09001, doi:10.1088/1748-0221/6/09/P09001, arXiv:1106.5048.

[56] CMS Collaboration, "Jet energy scale and resolution in the CMS experiment in pp collisions at 8 TeV", *JINST* **12** (2017) P02014, doi:10.1088/1748-0221/12/02/P02014, arXiv:1607.03663.

[57] CMS Collaboration, "CMS luminosity measurements for the 2016 data-taking period", CMS Physics Analysis Summary CMS-PAS-LUM-17-001, 2016.

[58] CMS Collaboration, "CMS luminosity measurements for the 2017 data-taking period at $\sqrt{s} = 13$ TeV", CMS Physics Analysis Summary CMS-PAS-LUM-17-004, 2017.

[59] CMS Collaboration, "CMS luminosity measurements for the 2018 data-taking period at $\sqrt{s} = 13$ TeV", CMS Physics Analysis Summary CMS-PAS-LUM-18-002, 2018.

[60] T. Junk, "Confidence level computation for combining searches with small statistics", *Nucl. Instrum. Meth. A* **434** (1999) 435, doi:10.1016/S0168-9002(99)00498-2, arXiv:hep-ex/9902006.

[61] A. L. Read, "Presentation of search results: the CL_s technique", *J. Phys. G* **28** (2002) 2693, doi:10.1088/0954-3899/28/10/313.

[62] The ATLAS Collaboration, The CMS Collaboration, The LHC Higgs Combination Group, "Procedure for the LHC Higgs boson search combination in Summer 2011", Technical Report CMS-NOTE-2011-005, ATL-PHYS-PUB-2011-11, 2011.